Acta Polytechnica CTU Proceedings **41**:1–7, 2023
https://doi.org/10.14311/APP.2023.41.0001

Published by the Czech Technical University in Prague

STEREOLITHOGRAPHY FOR MANUFACTURING OF ADVANCED POROUS SOLIDS

Veronika Drechslerová[a,*], Michaela Neuhäuserová[a], Jan Falta[a], Jan Šleichrt[a], Daniel Kytýř[b]

[a] *Czech Technical University in Prague, Faculty of Transportation Sciences, Department of Mechanics and Materials, Na Florenci 25, 110 00 Prague 1, Czech Republic*

[b] *Czech Academy of Sciences, Institute of Theoretical and Applied Mechanics, Prosecká 809/76, 190 00 Prague 9, Czech Republic*

[*] corresponding author: drechver@fd.cvut.cz

Abstract. The aim of this paper is focused on benefits of stereolithography (SLA) technology for the fabrication of the lightweight lattice structures with potential for load-bearing function and high absorption of impact energy. SLA is an additive manufacturing technology employing the principle of liquid resins curing moderated by radiation of a wavelength from ultra-violet band where resulting material parameters are tunable by setting of the curing process. The batches of samples manufactured using three different resins were subjected to quasi-static uni-axial tensile and compression tests. Acquired data were processed to derive deformation behaviour expressed as stress-strain diagrams and fundamental material properties. Based on the knowledge obtained from the mechanical tests, the setup of the fabrication parameters, the most suitable resin for manufacturing of the lattice structures and the overall suitability of SLA technology for the fabrication of advanced porous materials, were determined.

Keywords: Stereolithography, advanced porous materials, quasi-static testing, resin, mechanical characteristics.

1. Introduction

In recent decade, additive manufacturing technologies attract the attention of researchers and producers all over the world opening completely new areas of possibilities in structural design and material engineering [1]. It allows the production from metallic lightweight and high strength structures to nano-level bioprinting for tissue engineering purposes [2–4].

Stereolithography (SLA) is an additive manufacturing technology originally patented (US4575330A) by Chuck Hull in 1984 [5]. SLA works on the principle of curing a liquid photosensitive resin layer-by-layer using a light source – a projector or an ultraviolet laser beam with a typical wavelength range 300–400 nm [6]. The light source in a predefined path hits the surface of the photosensitive liquid and forms a new layer by selective curing. The process is repeated until the entire sample is finished. Final products are post-treated by UV light source to reach required and time stable mechanical properties.

One of the SLA benefits is a good ratio of the resolution compared to the size of the produced part and speed of the printing. This fact is very important for design of complex lattices structures, e.g., auxetics requiring advantageous materials properties such as low density, high energy absorption, resistance to dynamic loading and fatigue, and high toughness [7, 8].

Compared to conventional materials, auxetic materials expand laterally during stretching and shrink during compression. This principle of behaviour is known as the auxetic effect and causes materials to exhibit superior mechanical properties. As a result of the given deformation behavior, auxetic materials have a negative Poisson's number, which is defined as the negative ratio between the transverse ϵ_y and longitudinal ϵ_x deformation of the material under load [7]. The deformation behaviour of auxetic materials is caused by their specific internal structure, which is formed by modifying basic two-dimensional (2D) geometric shapes such as hexagons, triangles or squares [9, 10].

SLA is still a relatively new technology with significant effect of resin material and curing parameters to the primary load bearing function and the deformation behaviour of the structure. To quantify this effects and optimization fabrication parameters the experimental campaign including in total of 54 samples was carried out consisting of quasi-stating tensile testing of bulk material and compression testing of the lattice structure. Based on acquired data basic mechanical properties of each material used were calculated. From the results obtained, the most suitable material for the production of advanced porous materials and the auxetic 3D structure that showed the highest resistance to compression loading was determined.

2. Materials and methods

2.1. Sample preparation

For the quasi-static tensile loading, dog bone shape specimens were developed according to ASTM D638-14 standard. The standard defines four types of specimens, and this work was based on the Type II specimen (see Figure 1), which is suitable for material thicknesses of 7 mm or less. The test specimen was designed with a thickness of 4 mm and its dimensions are shown in Table 1. The model was designed using Inventor Professional 2022 (Autodesk Inc., USA) and printed at two different angles, see Figure 1, to investigate the effect of different layer orientation during printing on its mechanical properties:

- the specimen was rotated 90° about the x-axis, with the specimen perpendicular to the platform;
- the specimen was rotated 60° about the x-axis.

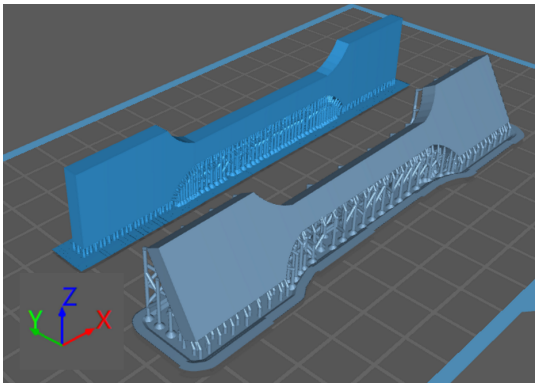

Figure 1. Design and orientation of the specimens for tensile test.

Parameter	Dim. [mm]
Overall length L	115
Gauge length L_0	40
Gauge width W	6
Thickness T	4
Curvature radius R	14

Table 1. Dimensions of the tensile test specimen.

For quasi-static compression loading, samples of 3D auxetic structures composed of elementary 2D re-entrant hexagonal honeycomb cells were created. The structures were designed in four variants differing from each other in the number of cells in the structure and the thickness of the cell struts, and for all designs, a top and bottom contact faces of 0.6 mm thickness was created to ensure a good distribution of the loading force during the specimen measurements. The different designs and dimensions of the structures are listed in Table 2 and depicted in Figure 2. The auxetic structures were printed in a 30° rotation about the x and y-axes, with the structure placed on removable supports.

2.2. Materials

Three different resins compatible with the Sonic Mighty 4K (Phrozen, Taiwan) printer were chosen to produce the specimens to demonstrate the dispersion of resulting material properties. Aqua Blue and ABS-like Matte Gray (Phrozen, Taiwan) resins were chosen mainly for their high printing accuracy and low toxicity. The samples manufactured from mentioned materials achieve high hardness and toughness. Geometry reliability is higher compared to the other resins. This is due to their very low viscosity. The advantage of UV DLP Firm Grey (Photocentric Inc., USA) resin is its strength with low yielding under high stress. This property is widely used for the manufacture of components that must not be brittle and where high load capacities are required. Printed models exhibit low flexibility but very high toughness, durability and longevity.

2.3. Setting production parameters

Appropriate setting of production parameter values has a crucial effect on the accuracy and overall success of the print. The individual parameters were set using CHITUBOX 1.7.0 proprietary software compatible with the printer. The setting of the individual print parameters is closely linked to the choice of resin, so it was necessary to set the parameters for each of the three resins used separately and test their suitability when printing the calibration matrices. The printing parameters include, e.g., layer height, curing time of the lower and normal layers, lifting speed of the printer's build plate. The resulting print parameter values for each resin are listed in Table 3. In addition to the appropriate choice of values of individual parameters, it is also necessary to place support structures in critical areas of the model (overhangs, complicated shapes) to maintain a smooth printing process without deformation or damage of the printed object. The support structures form the basis for attaching layers of uncured resin in areas where there are no previous cured layers and blank printing would occur.

2.4. Samples post-treatment process

The sample production process did not end with the completion of printing. The prints already had their form but required post-treatment (cleaning, curing, removal of supports) to achieve the final mechanical properties. The printed samples first had to be suitably separated from the printer platform, using the plastic spatula. Thereafter the samples had to be stripped of residual uncured resin. After the water rinsing, an isopropyl alcohol ultrasonic bath was used for clearing of the fine structure. The cleaning time was set to 5 min and the heating temperature to 35 °C. The Cure Luna (Phrozen, Thaiwan) UV lamp was

Design –	**Number of cells** –	**Strut thickness** [mm]	**Dimensions** ($W \times D \times H$) [mm]
1	4×3	0.6	$15.00 \times 15.00 \times 16.20$
2	6×4	0.5	$15.00 \times 15.00 \times 16.00$
3	6×4	0.3	$15.00 \times 15.00 \times 16.00$
4	8×6	0.3	$15.00 \times 15.00 \times 16.00$

TABLE 2. Design parameters of the samples for compression testing.

Parameters	**Units**	**Resines**		
		Phrozen aqua	**Phrozen ABS-like**	**UV DLP firm**
layer height	[mm]	0.05	0.05	0.05
number of bottom layers	[–]	4	4	4
number of transition layers	[–]	0	0	0
transition type	[–]	linear	linear	linear
exposure time	[s]	2.5	2	6
exposure time of lower layers	[s]	30	30	80
light-off delay	[s]	11	11	9
light-off delay for lower layers	[s]	11	11	9
platform lift distance	[mm]	6	6	5
platform lift distance for lower layers	[mm]	8	8	6
lifting speed	[mm min^{-1}]	60	60	80
lifting speed for bottom layers	[mm min^{-1}]	60	60	80

TABLE 3. Settings for manufacturing procedure..

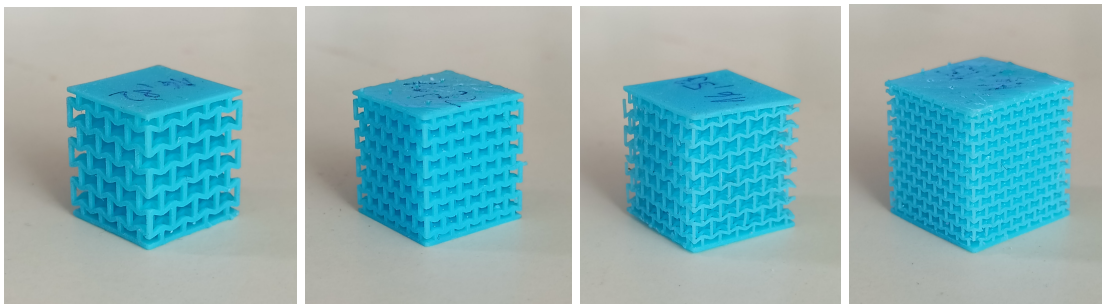

FIGURE 2. All types of auxetic structures (Design 1-4) according to Table 2 for compression testing.

used for subsequent curing of the samples. The curing time was set at 120 min to cure the samples throughout. A fully cured sample was plainly recognized by the change in its surface.

2.5. EXPERIMENTAL PROCEDURE

The printed test specimens were subjected to quasi-static tensile and compressive loading for subsequent determination of their mechanical characteristics. Three samples from each batch were tested for each resin. The test specimens were weighed before being measured separately and their initial dimensions were recorded for later calculations of mechanical property values.

The tensile test was carried out on the Instron 3382 (Instron Inc., USA) universal testing machine (see Figure 3). The tested specimen was placed in the clamps and subjected to the uni-axial tension at a loading rate of 0.5 mm min^{-1} until the failure, with a sampling rate of 100 Hz. During the test, the absolute elongation of the test specimen ΔL was recorded depending on the applied axial loading force F. After the loading was completed, the specimen was remeasured to determine its length after the failure.

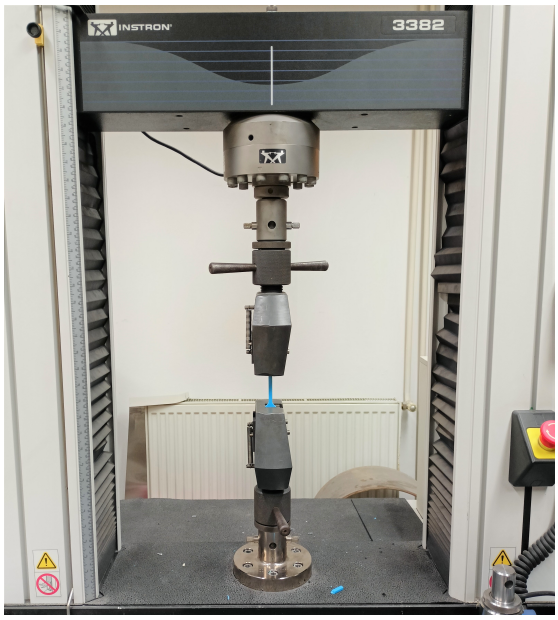

Figure 3. Tensile test arrangement.

Figure 4. Compression test arrangement.

For compression testing of the lattices samples an in-house table-top loading device [11] depicted in Figure 4 with nominal capacity of 3 kN and 2 μm positioning accuracy with read-out frequency of 200 Hz provided by LinuxCNC based control system [12]. A load cell with a capacity of 1 kN was used for the structures with a strut thickness of 0.3 mm and a load cell with a capacity 2 kN was used for the other two structures with strut thicknesses of 0.5 mm and 0.6 mm. The measurements were carried out at the loading rate of 2 mm min^{-1}. All the tested samples were compressed up to 50 % deformation. After reaching this strain value, the measurement was stopped.

2.6. Data Evaluation

The evaluation of the acquired data was carried out using MATLAB (MathWorks, Inc., USA), where an automatic script was created to calculate the basic mechanical properties and to obtain data for the production of stress-strain diagrams. First, the experimentally obtained data (namely, the load force record F and the absolute elongation of the specimen ΔL) were loaded automatically and other values such as the initial gauge length L_0, the length of the specimen after breaking L_u and the specimen cross-sectional area parameters A_C were manually entered. Based on these data, the stress vector σ and strain ϵ were determined according to the formulas

$$\sigma = \frac{F}{A_\mathrm{C}} = \frac{F}{T \cdot W}, \tag{1}$$

$$\epsilon = \frac{\triangle L}{L_0}. \tag{2}$$

Subsequently, a temporary stress-strain diagram was created and the data range corresponding to the linear region of the diagram was defined to determine the Young's modulus of elasticity in tension. The directive of the linear region was further used to construct a parallel to this region in determining the value of the yield stress σ_Y in tension, which was determined as the intersection of the directive with the constructed parallel. Furthermore, the tensile strength σ_U was evaluated according to the relation

$$\sigma_\mathrm{U} = \frac{F_{\mathrm{max_T}}}{A_\mathrm{C}}, \tag{3}$$

and ductility

$$D = \frac{L_\mathrm{u} - L_0}{L_0} \cdot 100. \tag{4}$$

Finally, standard deviations were calculated and stress-strain diagrams were generated using open source project for scientific data visualization Gnuplot [13]. During the compression test evaluation, the compressive stress-contraction and relative strain were calculated and subsequently inserted into the stress-strain contract diagrams to better understand the loading behaviour of each auxetic structure, and the porosity υ of the 3D printed structures from each resin was calculated according to the formula

$$\upsilon = \frac{V_\mathrm{t} - V_\mathrm{p}}{V_\mathrm{t}} \cdot 100, \tag{5}$$

where V_t is the total volume of the structure without pores and V_p is the volume of the structure with pores.

3. Results

3.1. Tensile testing

After evaluating the tensile tests of all the tested samples, the obtained values were averaged and resulting

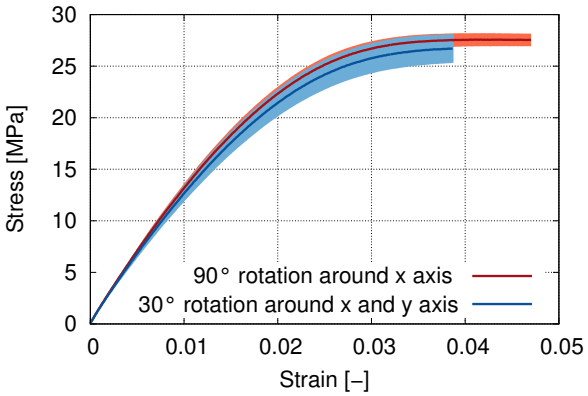

FIGURE 5. Tensile: Stress-strain diagram for specimens made from ABS.

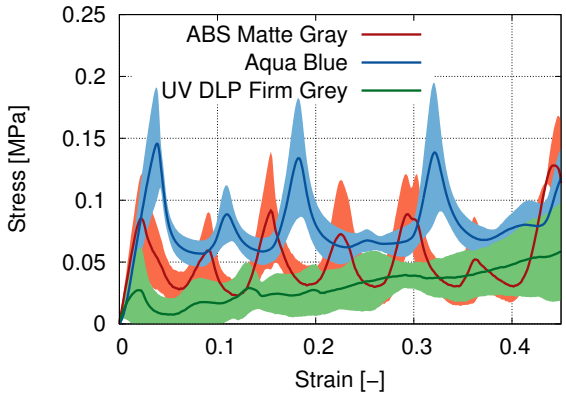

FIGURE 6. Stress-strain diagram for structures with 6×4 cells and thickness of 0.3 mm.

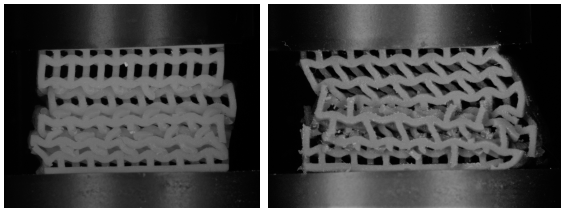

FIGURE 7. Detail of deformed structures.

in values of the basic mechanical characteristics. The results are summarized in Table 4.

The highest Young's modulus in the tension of all the used resins is for the samples made from the Phrozen Aqua Blue resin (AqB), while the sample with a 90° degree rotation around the x-axis is slightly higher. The AqB also has the highest yield strength σ_Y, strength σ_U, and nominal relative elongation at break ϵ_{tb}, which implies that the linear elastic deformation region is longer than for other resins and a higher loading force is required to induce plastic deformation and failure of the sample. The values obtained were compared with the data reported by the manufacturer and the data were found to be in disagreement with each other. It was also found from the stress-strain characteristic that the specimens made from UV DLP Firm resin (DLP) exhibit significant large plastic deformations compared to Phrozen ABS-like resin (ABS).

There was no significant effect of sample rotation during printing on deformation characteristics in terms of ultimate stress (see Figure 5). Test samples rotated during printing by 90° about the x-axis achieve larger strains than samples that were rotated by 60° about the x-axis.

3.2. Compressive testing

During the evaluating the compression test, it was necessary to calculate the porosities of the 3D auxetic structures to compare the deformation behaviour of the different auxetic structures (shown in Table 5). From the stress-strain diagrams it was found that the samples of all auxetic structures made from AqB and ABS resisted the compression loading better than the samples made from DLP, i.e. they achieved higher values of ultimate stresses. This phenomena can be observed in Figure 6, which shows a stress-strain diagram for a selected structure with the number of cells per face 6×4 and with the 0.5 mm thickness of the strut. The individual stress increases and decreases in the diagram show the progressive deformation of the layers of the structure. Due to the chosen high overall strain of the structure, which was 50 %, a high stress increase can be observed as the reason for the mutual contact of collapsed layers. Furthermore, from the developed contraction diagrams it was possible to see the different behaviour of the structures under loading depending on the used resin. While the structures made from Phrozen resins clearly show the stress increases and decreases associated with the layer-by-layer deformation of the structure, the DLP resin exhibited load distribution throughout the structure and deformation of the structure as a whole. The different modes of deformation of the structures are shown in Figure 7.

When comparing the effect of the thickness of the struts on the mechanical properties, it was found that for a structure with the same number of cells and made of the same resin, there is a rapid increase in stress with increasing thickness of the struts. As a result of the different thickness of the struts, the porosity of the structures within the same resin varied by 26 % for AqB, 16.82 % for ABS, and 19.65 % for DLP resins.

Although 4×3 and 8×6 structures showed almost identical porosity values, their behaviour under loading was influenced not only by the number of cells but also by the thickness of the struts. The struts with a higher thickness exhibits higher stiffness and the structure collapsed in shear bands amoung the layers. As the thickness of the struts decreased, the struts became more compliant and less brittle behaviour of the structure occurred (see Figure 8).

Different behaviour was observed on the individual structures after unloading. The structures made from DLP showed extensive plastic deformation during load-

Specimen position	Resin	Mechanical characteristic			
		E [MPa]	σ_Y [MPa]	σ_U [MPa]	ϵ_{tb} [%]
x and y axis rot. 30 °	AqB	1246.55 ± 22.39	30.80 ± 0.67	43.75 ± 1.32	3.22 ± 1.06
x and y axis rot. 30 °	ABS	809.71 ± 31.48	17.53 ± 0.63	26.85 ± 1.32	2.93 ± 0.93
x and y axis rot. 30 °	DLP	212.94 ± 16.52	5.20 ± 0.17	13.05 ± 0.95	1.46 ± 0.76
x axis rot. 90 °	AqB	1318.02 ± 23.35	32.80 ± 1.91	46.66 ± 1.66	3.56 ± 0.52
x axis rot. 90 °	ABS	867.09 ± 29.55	17.95 ± 0.52	28.35 ± 0.64	2.11 ± 0.49
x axis rot. 90 °	DLP	178.64 ± 16.95	4.50 ± 0.00	11.51 ± 0.69	1.47 ± 0.82
manufacturer data	AqB	588	–	24	–
manufacturer data	ABS	116	–	10	–
manufacturer data	DLP	700	–	26	–

Table 4. Tensile test mechanical characteristic values

Resin	Overall porosity [%]			
	4×3 0.6 mm	6×4 0.5 mm	6×4 0.3 mm	8×6 0.3 mm
AqB	64.69	52.28	78.33	62.68
ABS	70.43	65.40	82.22	69.15
DLP	71.98	62.84	82.49	69.17

Table 5. Porosity of 3D printed structures.

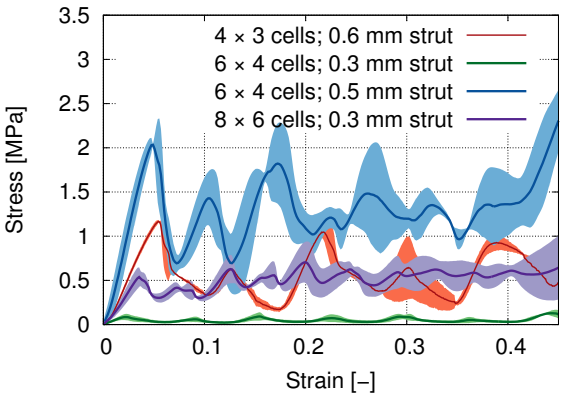

Figure 8. Comparison of different types of ABS auxetic structures.

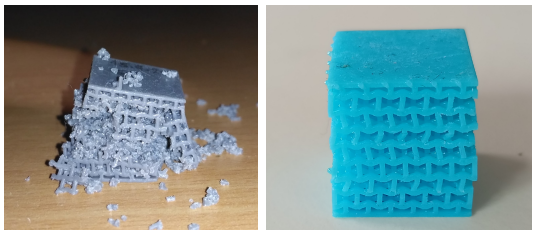

Figure 9. Damage of samples after loading – 6×4 structure with 0.5 mm strut thickness made of DLP (left), 6×4 structure with 0.5 mm strut thickness made of AqB (right).

ing. Samples of structures made from AqB and ABS showed much better resistance to permanent deformation. For the structures with a strut thickness of 0.3 mm, only minor plastic deformation was observed after unloading and they were almost able to return to their original form. For the other two structures with strut thicknesses of 0.5 mm and 0.6 mm, larger plastic deformations manifested by broken struts were observed, but despite this the structures were able to maintain their integrity. The structures after unloading are shown in Figure 9.

4. Conclusions

A prerequisite for successful SLA printing was the appropriate setting of production parameter values, which had a major impact on the accuracy of printing and its quality. Subsequently, test samples were printed and subjected to quasi-static tensile and compression loading. Measured data were presented in form of stress-strain diagrams and basic mechanical properties were calculated. Based on the performed tests, it was found that the most suitable material for the production of the auxetic structures was Aqua Blue resin produced by Phrozen. Its mechanical characteristics reached the highest values and the auxetic structures made from this resin exhibit lower brittleness. Among the loaded auxetic structure samples, the structure with 6×4 cells and 0.5 mm strut thickness showed the highest value of compressive strength and the highest ultimate stress of all tested structures. The structure deformed in layers and showed only minor plastic deformations after unloading.

Based on the performed experiment, it can be concluded that the stereolithography method for the fabrication of advanced porous structures appears to be suitable but depends on many variables, e.g., printer

setup, resin, the morphology of the specimen etc. The correct choice of the resin and the high printing accuracy of the 3D resin printer, which made it possible to print the designed complex geometry of the samples, led to this conclusion.

Acknowledgements

Financial support from the Operational Programme Research, Development and Education in the project INAFYM (CZ.02.1.01/0.0/0.0/16_019/0000766) and CTU internal project SGS21/131/OHK2/2T/16 are greatly acknowledged.

References

[1] G. Rasiya, A. Shukla, K. Saran. Additive manufacturing – A review. *Materials Today: Proceedings* **47**:6896–6901, 2021. International Conference on Advances in Design, Materials and Manufacturing, https://doi.org/10.1016/j.matpr.2021.05.181.

[2] N. Novak, O. Al-Ketan, M. Borovinšek, et al. Development of novel hybrid TPMS cellular lattices and their mechanical characterisation. *Journal of Materials Research and Technology* **15**:1318–1329, 2021. https://doi.org/10.1016/j.jmrt.2021.08.092.

[3] N. Novak, D. Kytýř, V. Rada, et al. Compression behaviour of TPMS-filled stainless steel tubes. *Materials Science and Engineering: A* **852**:143680, 2022. https://doi.org/10.1016/j.msea.2022.143680.

[4] G. Bouguéon, T. Kauss, B. Dessane, et al. Micro- and nano-formulations for bioprinting and additive manufacturing. *Drug Discovery Today* **24**(1):163–178, 2019. https://doi.org/10.1016/j.drudis.2018.10.013.

[5] L. D. Tijing, J. R. C. Dizon, I. Ibrahim, et al. 3D printing for membrane separation, desalination and water treatment. *Applied Materials Today* **18**:100486, 2020. https://doi.org/10.1016/j.apmt.2019.100486.

[6] I. Romero-Ocaña, S. I. Molina. Cork photocurable resin composite for stereolithography (SLA): Influence of cork particle size on mechanical and thermal properties. *Additive Manufacturing* **51**:102586, 2022. https://doi.org/10.1016/j.addma.2021.102586.

[7] N. Novak, M. Vesenjak, Z. Ren. Auxetic cellular materials – A review. *Journal of Mechanical Engineering* **62**(9):485–493, 2016. https://doi.org/10.5545/sv-jme.2016.3656.

[8] M. Benedetti, A. du Plessis, R. Ritchie, et al. Architected cellular materials: A review on their mechanical properties towards fatigue-tolerant design and fabrication. *Materials Science and Engineering: R: Reports* **144**:100606, 2021. https://doi.org/10.1016/j.mser.2021.100606.

[9] K. K. Saxena, R. Das, E. P. Calius. Three decades of auxetics research - materials with negative Poisson's ratio: A review. *Advanced Engineering Materials* **18**(11):1847–1870, 2016. https://doi.org/10.1002/adem.201600053.

[10] R. Zhong, X. Ren, X. Yu Zhang, et al. Mechanical properties of concrete composites with auxetic single and layered honeycomb structures. *Construction and Building Materials* **322**:126453, 2022. https://doi.org/10.1016/j.conbuildmat.2022.126453.

[11] T. Fíla, J. Šleichrt, D. Kytýř, et al. Deformation analysis of the spongious sample in simulated physiological conditions based on in-situ compression, 4D computed tomography and fast readout detector. *Journal of Instrumentation* **13**(11):C11021–C11021, 2018. https://doi.org/10.1088/1748-0221/13/11/c11021.

[12] V. Rada, T. Fíla, P. Zlámal, et al. Multi-channel control system for in-situ laboratory loading devices. *16th Youth Symposium on Experimental Solid Mechanics, YSESM 2018* **18**:15–19, 2018. https://doi.org/10.14311/APP.2018.18.0015.

[13] Gnuplot. [2022-10-05], http://www.gnuplot.info/.